Estimation of the ear canal displacement field due to in-ear device insertion using a registration method on a human-like artificial ear

S. Benacchio [a, b, c], O. Doutres [a], A. Le Troter [d,e], A. Varoquaux [d,e], E. Wagnac [a,c], V. Callot [d, e], F. Sgard [b]

[a] École de technologie supérieure, 1100 Rue Notre-Dame O, Montréal, QC, H3C 1K3

[b] Institut de recherche Robert-Sauvé en santé et sécurité du travail, 505 Boulevard de Maisonneuve O, Montréal, QC, H3A 3C2

[c] Centre de recherche de l'Hôpital du Sacré Coeur de Montréal, 5400 Boulevard Gouin O, Montréal, QC, H4J 1C5

[d] Aix Marseille Université, CNRS, CRMBM UMR 7339,Marseille, France

[e] APHM, Hôpital de la Timone, Pôle d'imagerie médicale, CEMEREM, Marseille, France

Abstract

Passive and active in-ear devices (IED) occluding the ear canal are commonly used to (i) protect people from high noise levels (earplugs), (ii) assist people suffering from hearing impairment (hearing aids) or (iii) help people in listening from their sound systems (earbuds). However, the usability and/or efficiency of IEDs can be greatly affected by several discomfort components (physiological, acoustical and functional). The mechanical pressure exerted by the IED onto the ear canal walls is greatly suspected to affect the aforementioned comfort components. This physical characteristic is closely related to the displacement field induced by the IED insertion, which has to be known for a better understanding of perceived discomfort. Thus, this paper proposes to validate a method based on medical images to estimate the displacement field of the ear canal walls due to the insertion of an IED. The approach is validated on a human-like artificial ear with canal geometry deformed using two custom molded IEDs with controlled shapes. These geometries are obtained using computed tomography imaging and the displacement field is computed using a

registration method. The errors due to the ear canal segmentation and to the registration steps are small enough to compute a relevant estimation of the expected displacement field. Results show that the amplitude of the displacement and its location into the ear canal can be evaluated with an accuracy of +/- 0.2 mm and +/- 0.4 mm respectively. Preliminary results on images with a degraded resolution indicate that the proposed approach used to assess the displacement field of the ear canal walls using computed tomography images could be applied on magnetic resonance images, which is a preferred method to image human subject ear canals for future investigations.

Keywords

Ear canal, deformation, displacement, earplug, hearing aids, earbud

Introduction

Passive and active intra-auricular devices occluding the ear canal, referred to as in-ear devices (IED) in this paper, are commonly used to protect people from high noise levels (earplugs), assist people suffering from hearing impairment (hearing aids) or help people in listening from their sound systems (earbuds). A common specification for all of these IEDs is related to the quality of the mechanical seal at the ear canal/IED interface that should ensure a good positioning of the IED with time. Another important specification shared by most of the IEDs is related to the quality of the acoustic seal at the ear canal/IED interface that should insulate adequately the eardrum from external noise. However, the usability and/or the efficiency of such devices can be limited by three major discomfort components also related to the quality of the mechanical and acoustic seals : (i) the physiological comfort component characterized by attributes such as friction, irritation or the mechanical pressure exerted by the device on the body, (ii) the acoustical comfort component characterized by attributes such as over- or under- attenuation of external noise, difficulty in communication, occlusion effect or acoustical feedback and (iii) the functional comfort component characterized by

attributes such as the ease of insertion or the looseness of the fit (French-Saint, et al., 1978; Casali, et al., 1987; MacKenzie, et al., 1989; Park, et al., 1991; Harrison, 1993; Azeres, et al., 2008; Kochkin, 2000; Pirzanski, et al., 2004; Davis, 2008; Conrad, et al., 2013; Davis, et al., 2016; Doutres, et al., 2017).

A factor that is greatly suspected to affect all three aforementioned comfort components is the deformation applied by the IED on the ear canal walls (Darkner, et al., 2007; Darkner, et al., 2008; Baker, et al., 2010; Norris, et al., 2012). However, the investigation of this deformation is not trivial. Direct measurement techniques are unpractical since they would require miniature displacement sensors onto the ear canal walls. Moreover, these sensors should deliver the 3D deformation field without affecting the mechanical coupling at the ear canal/IED interface. Indirect techniques based on the analysis of the shape modifications of a deformable solid due to an external load seem more appropriate to investigate ear canal deformations. In the specific application of an occluded ear canal, the initial shape corresponds to the geometry of the open ear canal and the modified shape, the one of the occluded ear canal. According to the authors' knowledge, the determination of the ear canal displacement field due to IED insertion has never been proposed in the past. A couple of studies have used indirect techniques to evaluate the ear canal deformation due to the jaw motion from two different perspectives : comfort (Grenness, et al., 2001; Darkner, et al., 2007) and energy harvesting (Delnavaz, et al., 2013; Delnavaz, et al., 2014; Carioli, et al., 2016). In these studies, the regions of maximum displacement between the open and closed mouth were evaluated using 3D scans of ear impressions obtained for both jaw positions and analyzed to get geometrical parameters of the ear canal (e.g., diameter, curvature, torsion and aspect ratio) (Delnavaz, et al., 2013; Delnavaz, et al., 2014; Carioli, et al., 2016) or to get 3D displacement field using a non-rigid registration technique (Darkner, et al., 2007).

The approach proposed by Darkner et al. (Darkner, et al., 2007) can be applied to the open/occluded ear canal if both geometries are captured from medical images. Indeed, ear impression cannot be used to evaluate ear canal deformation due to IED insertion since (i) it will deform the ear canal (even slightly) and thus prevent the acquisition of the open ear canal geometry and (ii) it will prevent the acquisition of the ear canal geometry for an occlusion by any type of IED. Furthermore, acquiring the shape of the ear canal from medical images in place of using a 3D scan of an ear impression allow (i) avoiding any bias associated with non-uniform contact between the ear canal and the ear impression, (ii) imaging of the entire ear canal from its entrance to its tip and not only to the tip of the ear impression (Egolf, et al., 1993; Oliveira, 1997; Yu, et al., 2015, Darkner, et al., 2017) and (iii) observing the position of the IEDs inside the ear canal (Inoue, et al., 2011). A registration method can be used for assessing the 3D displacement field of the ear canal due to IED insertion using the open and occluded ear canal images as the source and target images respectively (Zitova, et al., 2003; Klein, et al., 2009, Avants, et al., 2011). However, before to be applied on real subjects, this approach must be validated by controlling the deformation applied into the ear canal and evaluating its accuracy and precision.

In this work, the proposed approach was applied to an artificial ear mimicking a real human ear. To precisely control the displacement applied to the ear canal, the artificial ear was successively occluded using two non-deformable acrylic custom molded IEDs. The first one was a custom molded earplug made up from an ear impression of the artificial ear. The second IED was identical to the first earplug but its geometry has been modified by gluing small beads controlled diameter (1.9 mm) on it. Computed tomography (CT) images of the artificial ear occluded by the two aforementioned IEDs were performed. A registration method was used to obtain the displacement field between these two occlusion cases in order to observe the geometry modification of

the ear canal due to the presence of the beads. The use of two occlusion conditions instead of an open and occluded ear canal was preferred because it was easier to locally control the dimensions of two beads rather than the geometry of a whole IED. To evaluate the accuracy of the method, the computed displacement was compared to the known diameter and position of the beads and similarity indices were used to evaluate the precision of the approach.

This paper is organized as follows. The design of the artificial ear and of the IEDs is detailed in the first section. Then, CT measurements and the obtained images are presented. The segmentation and registration steps applied to the obtained images to assess the displacement field due to the presence of the beads are detailed. The accuracy and the precision of these two steps are defined and the tools used to evaluate them are presented. Then, the resolution of images is degraded to mimic images obtained using magnetic resonance imaging (MRI). In the second section, computed results using the proposed approach are compared to the measured diameters of the beads and similarity indices are used to evaluate the accuracy and the precision of the method. The segmentation process is performed by different operators in order to evaluate the variability of the method. The proposed approach is also applied to images with MR-like resolution. In the end, these results are discussed in the third section.

1 Materials and Method

1.1 Controlled environment

1.1.1 The artificial ear

To finely control the deformation induced by the IEDs, the proposed method was validated on an artificial human ear. Measurements on an artificial ear are easier to perform than on a human subject. For example, an artificial ear is smaller than a human head and can easily be imaged using a small imaging apparatus (Micro-CT or MRI with

a reduced size of the antenna). Another advantage to use an artificial ear is that the image noise due to human subject movements during imaging is eliminated. As the artificial ear remains static, there is no such movement during acquisition. The anatomical structure of the ear can also be simplified using an artificial ear in order to make the image post-processing easier. However, the artificial ear must still closely mimic a real ear in order to be able to easily transfer the proposed approach on human subjects after validation. To obtain a realistic ear canal and surrounding tissue geometries, the artificial ear was reconstructed using magnetic resonance images acquired on a 28 years old male subject. The characteristics of the sequence used to image the ear canal of the subject are given in Table 1.

MR system	Siemens 3T (Verio)
Radiofrequency (RF) coil	Head 32 channels
Sequence	Space 3D
Weighting	T1
Plane	Axial
Slices	128
Resolution [mm]	0.6 isotropic
Acquisition time [min]	9

Table 1: Parameters of the MRI sequence used to develop the human-like artificial ear.

The left ear canal of the subject was inspected by an otolaryngologist to ensure there was no outer ear pathology. Then, the tissues surrounding the left canal of the subject were segmented on MR images using the software *MIMICS, Materialise (Leuven, Belgium)*. Three masks were used to differentiate the soft tissues (fat, muscles, skin...), the cartilage and the bone around the ear canal as shown in Figure 1.a. In this figure and in the following, the letters S, I, P, A, M and L refer to superior, inferior, posterior, anterior, medial and lateral respectively. Then, a numerical 3D reconstruction of the ear canal geometry with surrounding tissues was carried out. An approximately 70 mm high and 80 mm diameter cylinder was extracted from this model and is depicted in

Figure 1.b. This computer-aided design (CAD) model was used to build the artificial outer ear using 3D printing techniques with polyurethane based materials for soft tissues and cartilage and epoxy based ceramic composite for the bony part. The final artificial outer ear built by the company *True Phantom Solutions (Windsor, Canada)* is shown in Figure 1.c.

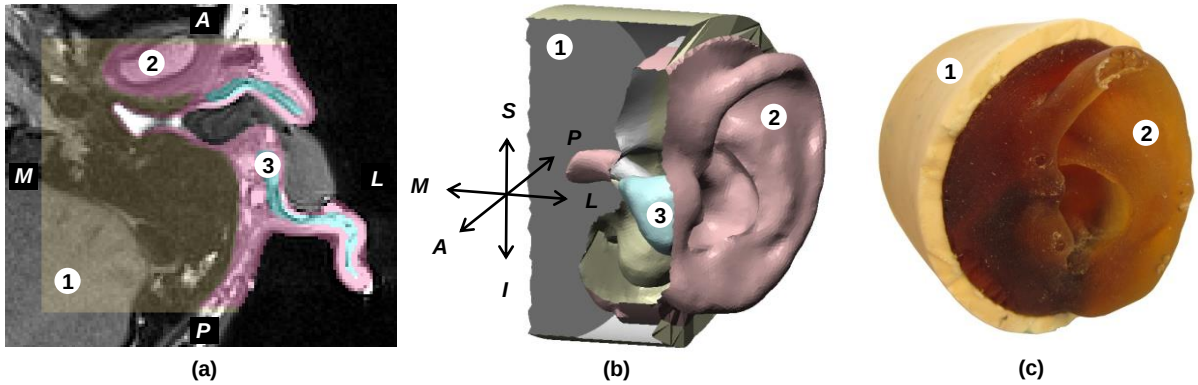

Figure 1: (a) Axial slice of the MR images used to segment the bony part (1), soft tissues (2) and cartilage (3). (b) Numerical model and (c) final artificial ear built by True Phantom Solutions (Windsor, Canada). The letters given with the coordinate system refer to superior (S), inferior (I), posterior (P), anterior (A), medial (M) and lateral (L) respectively.

Since images of the occluded ear of the subject were used for the design of the artificial ear, the canal of the subject was deformed by an earplug used to protect him during MRI. However, the earplug was not segmented during the reconstruction step. Thus, the artificial outer ear represents the ear of the subject permanently deformed by the earplug. This ear canal is considered as a new ear with its own shape and its own rigidity set by the three materials used to approximate the mechanical and acoustical behavior of a real ear.

1.1.2 Custom molded in-ear devices

In order to estimate the accuracy and the precision of the method, two IEDs were manufactured. The first one was an acrylic custom earplug referred to as IED#1, fabricated from a usual silicone impression of the artificial ear canal and considered as non-deformable (see Fig. 2.a). The second IED was the same custom earplug with two beads glued on its surface. It is referred to as IED#2 in the following and is shown in Figure 2.b.

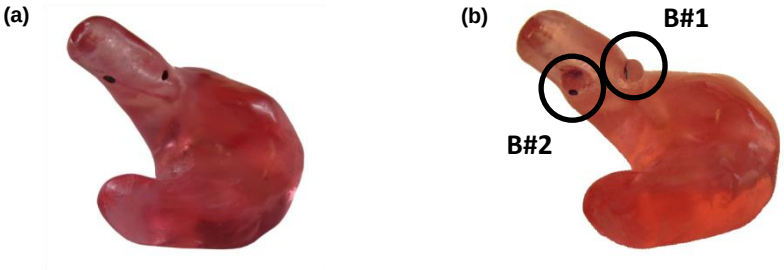

Figure 2: (a) Custom earplug (IED#1) and (b) modified custom earplug (IED#2). On the IED#2, beads are glued between the first and the second bend of the posterior part of earplug (B#1) and on the upper part of the second bend of earplug (B#2).

The beads have been positioned at two specific locations for which a good contact between the surface of the IED#1 (earplug without bead) and the walls of the ear canal was observed. These good contact locations were chosen where no air gap (appearing in black on images) was visible for images of the artificial ear occluded by the IED#1. The bead B#1 was glued between the first and the second bend on the posterior part of the earplug (see Fig. 2.b). The bead B#2 was glued on the upper part of the second bend of the earplug (see Fig. 2.b). The initial diameter of the beads was 2 mm. Then, they were truncated to create a flat surface, which was glued on the IED#2. The new height of the truncated beads was 1.9 mm. This dimension is still called diameter of the beads in the following for simplicity.

Since the beads were also considered non-deformable and much more rigid than the silicone mimicking the soft tissues in the artificial ear, the difference between the geometries of the ear canal occluded by IED#1 and IED#2 were only due to the two

beads. Hence, the proposed method will be considered as validated if the beads diameter and their locations in the ear canal can be recovered.

1.2 Ear canal imaging

The geometry of the artificial ear canal was imaged using a Nikon XT H 225 micro CT X-Ray Scanner with a 0.06 mm isotropic resolution. The image reconstruction from CT-scans was performed using the software *CT Pro 3D, Nikon Metrology (Brighton, United States)* and is shown in Figure 3.a. The obtained reconstruction is made of voxels whose gray levels depend on the depicted area of the artificial ear (soft tissues, cartilage and bone). Figure 3.b gives one coronal slice of this reconstruction.

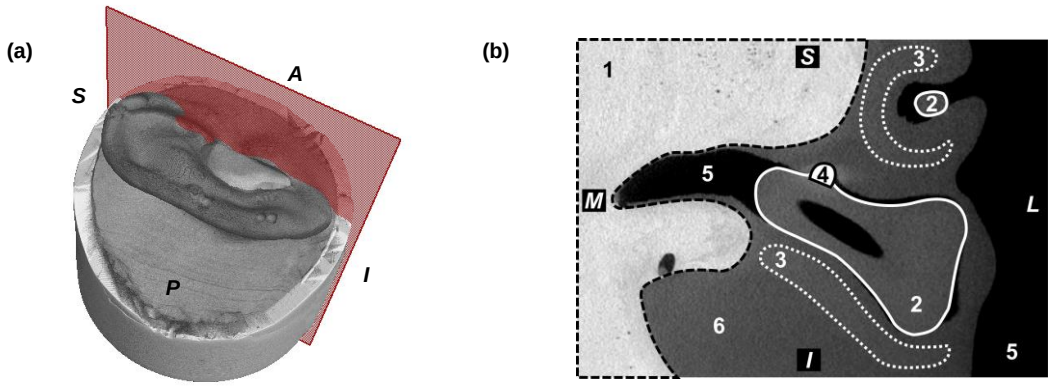

Figure 3: (a) 3D reconstruction of the occluded artificial ear from CT-scans measurements. The red plan indicates the cross section of the 2D view. (b) Coronal slice of the 3D reconstruction of the artificial ear. The regions delimited by the dashed black, solid white, dotted white and solid black lines are the bony part (1), the earplug (2), the cartilage (3) and the bead (4) respectively. The black part is the air (5) and the remaining dark gray part is the silicone mimicking the soft tissues (6).

In this figure, the air (5) is the black area, the bony part (1) is the light gray area, the soft tissues (6), cartilage (3) and earplug (2) are the medium gray areas and the visible bead B#2 (4) is the white area. Then, the 3D reconstruction was carried out in the software *VG-studio, Volume Graphics (Heidelberg, Germany)* from which a DICOM image set was exported. In the following, the term image refers to an entire DICOM stack of images. The images obtained for the artificial ear occluded by the IED#1 and the IED#2 were then used to compute the displacement field between these two occlusion cases.

1.3 Ear canal segmentation and registration

1.3.1 Segmentation

Before applying the registration method on images, it is noteworthy that the white voxels appearing in the artificial ear occluded by the IED#2 don't exist for the artificial ear occluded by the IED#1. This detail might bring some difficulties during registration since the beads are supposed to be a part of the IED#2 and should have the same gray value. Moreover, Figure 3.b shows that the gray values of the earplug and of the soft tissues are very close which also might bring some registration errors. To avoid such a registration error, it was necessary to segment the ear canal occluded by both the IED#1 and the IED#2. Thus, the air and the earplug in the case of the IED#1 and the air, the earplug and the beads in the case of the IED#2 were represented by one single volume with one global gray value as illustrated in Figure 4. Semi-automatic segmentation tools from the software *MIMICS, Materialise (Leuven, Belgium)* were used to perform the 3D segmentation of the artificial ear canal.

1.3.2 Registration

The general principle of the registration method is to apply a transformation model to a source (or moving) image in order to optimise its similarity with a target (or fixed) image. The source and target images correspond to the ear canal occluded by the IED#1 and IED#2 respectively. The deformed image corresponds to the source image deformed to match the target image. During registration, the similarity between images can be computed comparing the voxel gray values or the contrast between voxels in each image. A lot of transformation models and similarity metrics can be used to register images (Zitova, et al., 2003). In this paper, the transformation models and the similarity metrics implemented in the Advanced Normalization Tools (ANTs)[1] library

[1] https://github.com/stnava/ANTsDoc/raw/master/ants2.pdf *(last accessed 2017-12-21)*

toolkit were used to compute the registration steps. More specifically, a rigid registration and a deformable registration steps were performed to obtain the deformation of the ear canal. It is worth mentioning that one registration step can have several stages in order to improve the quality of the registration.

The rigid registration step is used to take into account that the imaged volume, in our case the artificial ear, has not the same position for two different acquisitions. Therefore, the resulting images are not orientated in the same way. To realign these images, the rigid registration only authorizes translations and rotations. In order to use as much details as possible and to obtain a global repositioning of the images, the entire artificial ear was used for the rigid registration step. Only one stage whose parameters are given in Table 2 was used for the rigid registration step.

Stage 1	
Transformation model	Rigid (linear)
Similarity metric	Mutual Information
Number of levels	4
Number of authorized iterations per level	1000x500x250x2
Convergence threshold and window size	10e-6, 10
Shrink factor per level	8x6x4x2
Sigma of gaussian smoothing per level	4x3x2x1 voxels

Table 2: Parameters for the rigid registration step.

Among these parameters, the similarity metric defines the way the similarity between two images is computed. For example, the mutual information metric compares the histograms of two images to check their similarity while the cross correlation metric checks whether the surrounding neighborhood of voxels are similar in each image. In the latter case, the radius corresponds to the number of voxels included in the surrounding neighborhood in each direction. The number of levels corresponds to the number of resolution levels used to compute the registration. The general idea of ANTs is to start the registration with low resolution and highly smoothed images. Then,

resolution is increased and the smoothing decreased level by level until the initial image resolution with no smoothing. Thus, each level of image details is used to compute the registration. The number of iterations per level defines the maximum iteration allowed during the computation for each level. The convergence window size indicates the maximum number of iterations the optimized parameter computed from the similarity metric has to remain under the convergence threshold before to step out of a level. The shrink factor defines the factor by which the resolution is divided for each level. The sigma of Gaussian smoothing defines the Gaussian function standard deviation used to reduce details and noise in images for each level.

Here, the mutual information metric was chosen since it was known as the best metric for linear registration before a deformable registration using ANTs (Avants, et al., 2011).

Once the source and target images had the same orientation, a region of interest (ROI) was defined and extracted from both images to reduce the number of voxels used for the deformable registration step. The choice of the ROI is important for deformable registration since this region must be large enough to avoid boundary effects and small enough to focus the computation efforts on a specific area. In this paper, a 30.54x34.85x49.10 mm (Coronal/Axial/Sagittal) parallelepipedic region surrounding the ear canal was chosen as ROI.

Then, deformable registration was applied to ROIs. In this case, the transformation model used for this registration authorizes the deformation of the image using a grid connecting together each neighbouring voxel. In order to increase the quality of the deformable registration step, two stages were performed with different parameters. Details of the transformation model and similarity metric used for the two stages of the deformable registration step are given in Table 3.

Stage 1	
Transformation model	Symmetric Normalization (diffeomorphic)
Similarity metric	Cross correlation (radius = 8 voxels)
Number of levels	5
Number of authorized iterations per level	200x200x200x200x200
Convergence threshold and window size	10e-6, 10
Shrink factor per level	6x5x4x3x2
Sigma of gaussian smoothing per level	6x5x4x3x2 voxels
Stage 2	
Transformation model	Symmetric Normalization (diffeomorphic)
Similarity metric	Cross correlation (radius = 10 voxels)
Number of levels	3
Number of authorized iterations per level	8x8x8
Convergence threshold and window size	10e-6, 10
Shrink factor per level	4x3x2
Sigma of gaussian smoothing per level	4x3x2 voxels

Table 3: Parameters for the deformable registration step

The cross correlation metric was chosen for deformable registration since it was believed to be the very robust (Avants, et al., 2008) and give good results compared to other metrics in this specific case.

It is worth mentioning that for the two stages of the deformable registration step, a final level was added and computed with a shrink factor equal to 1 but zero authorized iteration. This last level was used to keep the resolution of the deformed image equal to the resolution of the source and target images. An example of a deformable registration is presented in Figure 4 on a coronal slice of the artificial ear. After the deformable registration step, the transformation file computed during the registration of the source (Fig. 4.a) on the target (Fig. 4.b) images was applied to the source image in order to obtain the deformed image (Fig. 4.c). The transformation file was also used to compute the displacement field (Fig. 4.d) of the ear canal. As the displacement field is given for each direction of space, its magnitude is used in this paper and computed using the Euclidean norm. In Figure 4.d, the values of the displacement field magnitude

included between 0.6 and 2 mm are superimposed using a color scale on the source image.

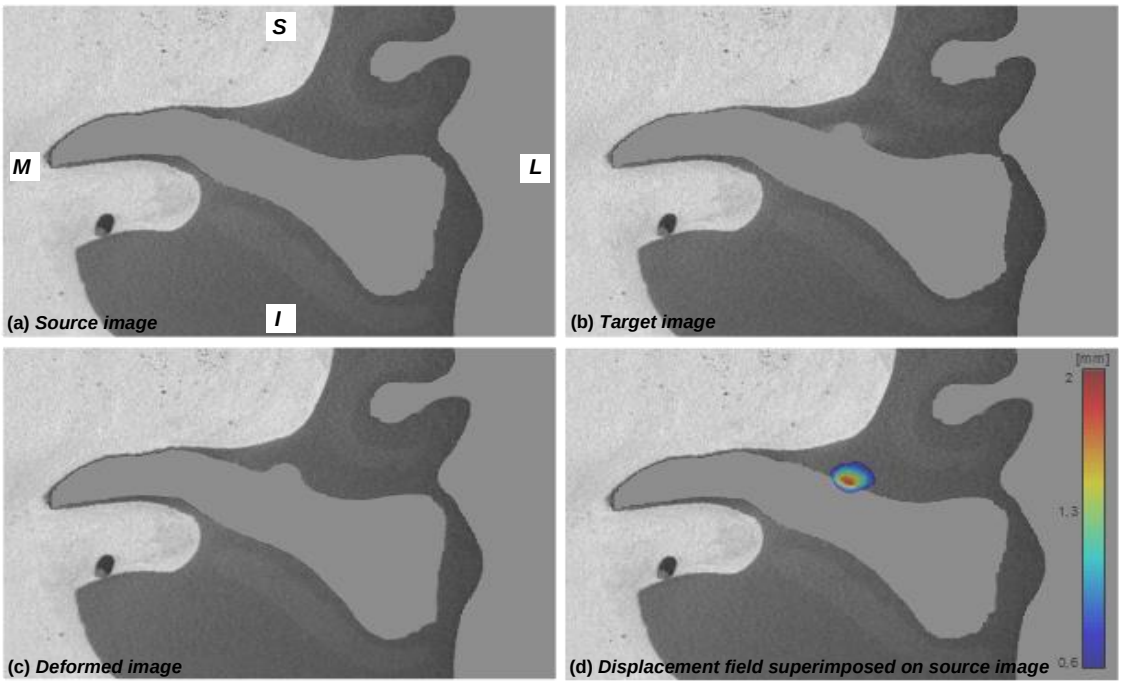

Figure 4: One coronal slice of the (a) source, (b) target and (c) deformed images and (d) computed displacement field superimposed using a color scale on the source image.

In the following and in order to identify the most deformed parts of the ear canal, the magnitude of the displacement field is projected along its walls. Ear canals are usually divided in cross sections perpendicular to their center line (Stinson, et al., 1989a; Stinson, et al., 1989b). In this paper, sagittal planes are used to divide the ear canal. The proposed representation doesn't give the deformation along the curvature of the ear canal but as a function of its depth from the end straight to the entrance. Examples of this representation are given in section 2.2.1. The bright shadow around the location of the bead in Figure 4.b is a radial artifact due to the high density of the bead. This effect is small enough to be preferred to the use of a softer material to ensure the high rigidity, and so the non deformable aspect of the beads.

1.4 Accuracy and precision

1.4.1 Segmentation

As the segmentation is known to be a sensitive point for the precision and the accuracy of the registration, this process was repeated by three operators. First, the operator 1 (OP#1) performed the segmentations of the ear canal occluded by the IED#1 and IED#2. Then, operators 2 (OP#2) and 3 (OP#3) performed both their own segmentation of the IED#1. The comparison of the three IED#1 segmentations with the non-segmented image gives information on the accuracy of the displacement field provided by the proposed approach. The comparison of the three IED#1 segmentations amongst themselves and of the resulting registrations using the IED#2 segmentation of the OP#1 as target gives information on the precision of the approach. The segmentation is considered accurate if any segmented volume provided by any operator is close to the geometry of the ear canal observed on the non-segmented image of the ear canal occluded by the IED#1. The accuracy of the segmentation could only be estimated visually and depends on (i) the resolution and the contrast of images and on (ii) the skills of the operators.

The segmentation is considered as precise when all segmented volumes provided by all operators are similar. The precision of the segmentation also depends on (i) the resolution and the contrast of images and on (ii) the skills of the operators. It was quantitatively evaluated using similarity indices comparing segmentations performed by all operators. Similarity indices, computed using the three IED#1 segmentations described earlier, are defined in details in section 1.4.3.

1.4.2 Registration

The rigid registration step was considered as accurate and precise since an excellent superposition of the non-deformed part (essentially the bony part) of the source and target images was observed. Thus, only the accuracy and the precision of the

deformable registration step were evaluated. The quality of this registration step was evaluated into the region of interest described in section 1.3.2

The deformable registration is considered as accurate if any estimated amplitude and location of the computed displacement are close to the real displacement of the ear canal. The accuracy of the deformable registration step depends on (i) the resolution and the contrast of images, (ii) the accuracy and the precision of the segmentation and (iii) the registration method and its input parameters. The accuracy of the deformable registration step was qualitatively evaluated by comparing the location of the maximum displacement in the ear canal with the location of the bead centers on the IED#2. A quantitative evaluation of the accuracy was performed by comparing the amplitude of the estimated displacement field and the diameter of the beads. The transformation file obtained thanks to the deformable registration was also applied to the segmented images of the ear canal to give the deformed segmentations. The latter were compared to the segmentations of the target image using similarity indices.

The deformable registration is considered as precise when all estimated amplitude and location of the displacement computed from images segmented by all operators are similar. The precision of the deformable registration step depends on (i) the accuracy and the precision of the segmentation and (ii) the registration method and its input parameters. The precision of the deformable registration step was quantitatively evaluated using similarity indices comparing the deformed images computed using segmentations of the three operators as source images.

1.4.3 Similarity indices

In order to estimate the segmentation and registration accuracy and precision, usual statistical values are used and presented here (Klein, et al., 2009).

- The *Dice index* was calculated using ear canal segmentations of the source, the target and the deformed images. This index is given as a mean overlap between

two segmentations. For example, if the overlap between the source image S and the target image T is considered, the dice index is given such as,

$$Dice\ Index = \frac{2\,|S \cap T|}{|S|+|T|},$$

where ∩ is the intersection between segmentations, and |.| the count of voxels equal to 1 in the segmentations.

The Dice index is equal to 1 for a perfect match between the two images. A Jaccard index could have been used to give similar information on the similarity between images. However, only the Dice index is presented in this paper for simplicity.

- *False positives* give the ratio of voxels of the source segmentation which do not correctly match the target segmentation. Thus, the lower the value, the better the registration. *False negatives* give the ratio of voxels of the target segmentation which are not correctly matched by the source segmentation. Their expressions are given by,

$$False\ Positive = \frac{|S \setminus T|}{|S|},$$

$$False\ Negative = \frac{|T \setminus S|}{|T|},$$

where \ is the set difference. For these two cases, the lower the ratio, the better the registration.

1.4.4 Registration noise

In order to evaluate the minimum displacement that the registration was able to compute, a fixed region was selected on the source and target images. A deformable registration was applied on this region and the obtained displacement is considered as the registration noise whose maximum value defines the minimum displacement that can be estimated using the proposed method.

1.5 Application to MRI-like resolution images

The use of a computed tomography method to image human subject can be problematic since it is an invasive way to obtain anatomical images. A safer and so preferred method would be to use MR imaging technique. However, the resolution obtained using MRI is much lower than the resolution of micro CT. It is not obvious that the results obtained using CT images can be reproduced with the same precision and accuracy using MR images. After preliminary measurements, it seemed possible to obtain MR images of the ear canal of a human subject with a sufficient contrast for the segmentation step with a 0.6 mm isotropic resolution (see Table 1 and Figure 1 for example). This resolution is 10 times lower than the resolution used to validate the proposed method. In order to estimate if this method could be used for such a resolution, the images of the artificial ear were degraded to reach a 0.6 mm resolution. Then, the method was applied again (by OP#1 only) following the process presented in sections 1.3.1 and 1.3.2. Since the resolution of images was different, the parameters used during the deformable registration step were adapted to obtain an accurate and precise deformed image. The used deformable registration step had four stages whose parameters are given in Table 4.

Shared parameters for each stage	
Transformation model	Symmetric Normalization (diffeomorphic)
Similarity metric	Cross correlation
Number of levels	1
Convergence threshold and window size	10e-6, 10
Shrink factor	1
Sigma of gaussian smoothing	1 voxels
Specific parameters	
Stage 1	
Radius for the cross correlation	15 voxels
Number of authorized iterations	50
Stage 2	
Radius for the cross correlation	13 voxels
Number of authorized iterations	20
Stage 3	
Radius for the cross correlation	11 voxels
Number of authorized iterations	20
Stage 4	
Radius for the cross correlation	9 voxels
Number of authorized iterations	20

Table 4: Parameters for the deformable registration step applied to degraded images.

2 Results

2.1 Segmentation

2.1.1 Accuracy

The accuracy of the segmentation step is qualitatively evaluated thanks to a visual control of the segmented images. Figures 5.a, 5.b and 5.c show respectively one coronal, sagittal and axial slice of the segmentations performed by operators OP#1, OP#2 and OP#3 superimposed on the associated source images.

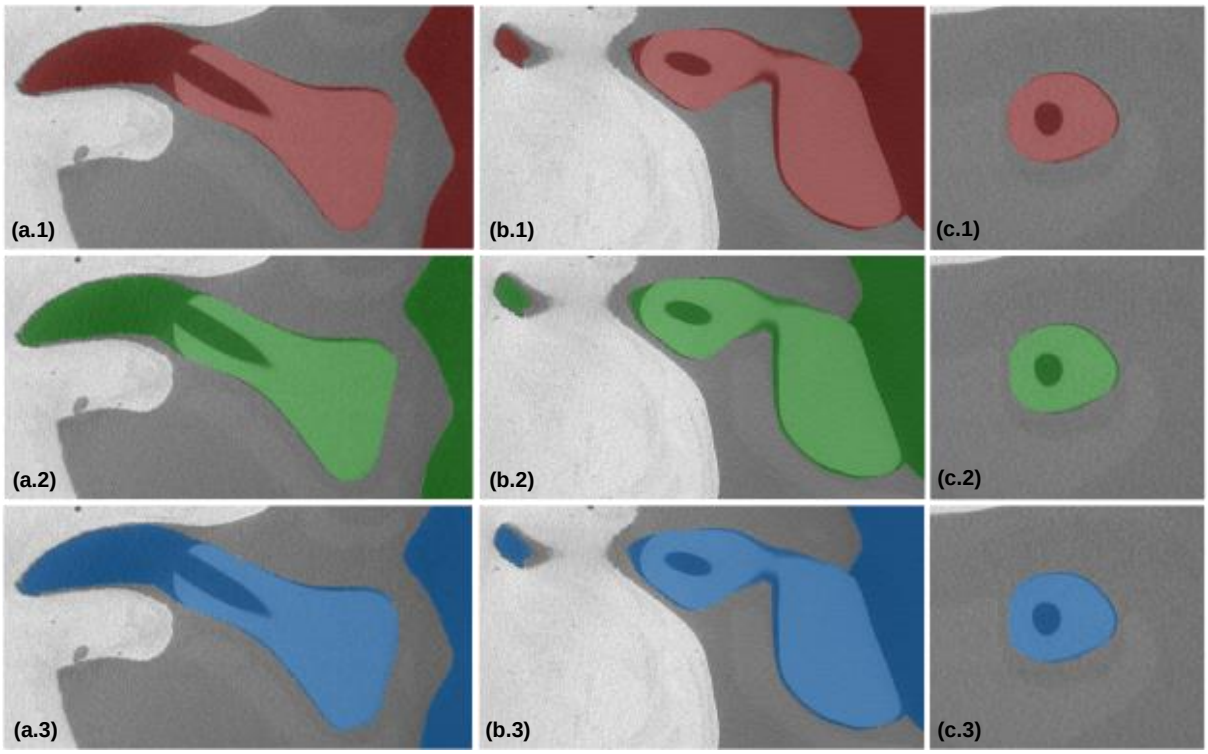

Figure 5: (a) Coronal, (b) sagittal and (c) axial views of the segmentations of the ear canal performed by OP#1 (red mask), OP#2 (green mask) and OP#3 (blue mask) superimposed on the corresponding source image.

As it is not possible to present all the slices of the segmented volume, only one slice in each view is presented here. However, according to these slices, the result of the segmentation step is accurate since the segmentations performed by each operator are close to the real geometry of the ear canal.

2.1.2 Precision

The precision of the segmentation step is quantitatively evaluated using the three segmentations to compute similarity indices given in Table 5.

	OP#1/OP#2	OP#1/OP#3	OP#2/OP#3	Mean (Stand. dev.)
Dice	0.995	0.994	0.993	0.994 (0.001)
False negative	0.003	0.004	0.004	0.004 (0.001)
False positive	0.007	0.007	0.011	0.008 (0.002)

Table 5: Similarity indices for the segmentations performed by the three operators.

These results confirm that the segmentation step is precise since the values of the Dice index are close to 1 and the values of false negatives and positives are close to 0.

2.2 Registration

2.2.1 Accuracy

To evaluate the accuracy of the deformable registration step, the computed displacement field is represented using a polar plot. This representation not only gives the amplitude but also a complete cartography of the displacement field inside the ear canal. Thus, it is possible to identify the region of maximum displacement applied on the walls of the ear canal and how much these regions are deformed. Figure 6 presents the surface plot of the ear canal walls displacement magnitude computed using the deformable registration parameters described in section 1.3.2 and using the segmentations performed by operator OP#1 (Fig. 6.b), OP#2 (Fig. 6.c) and OP#3 (Fig. 6.d).

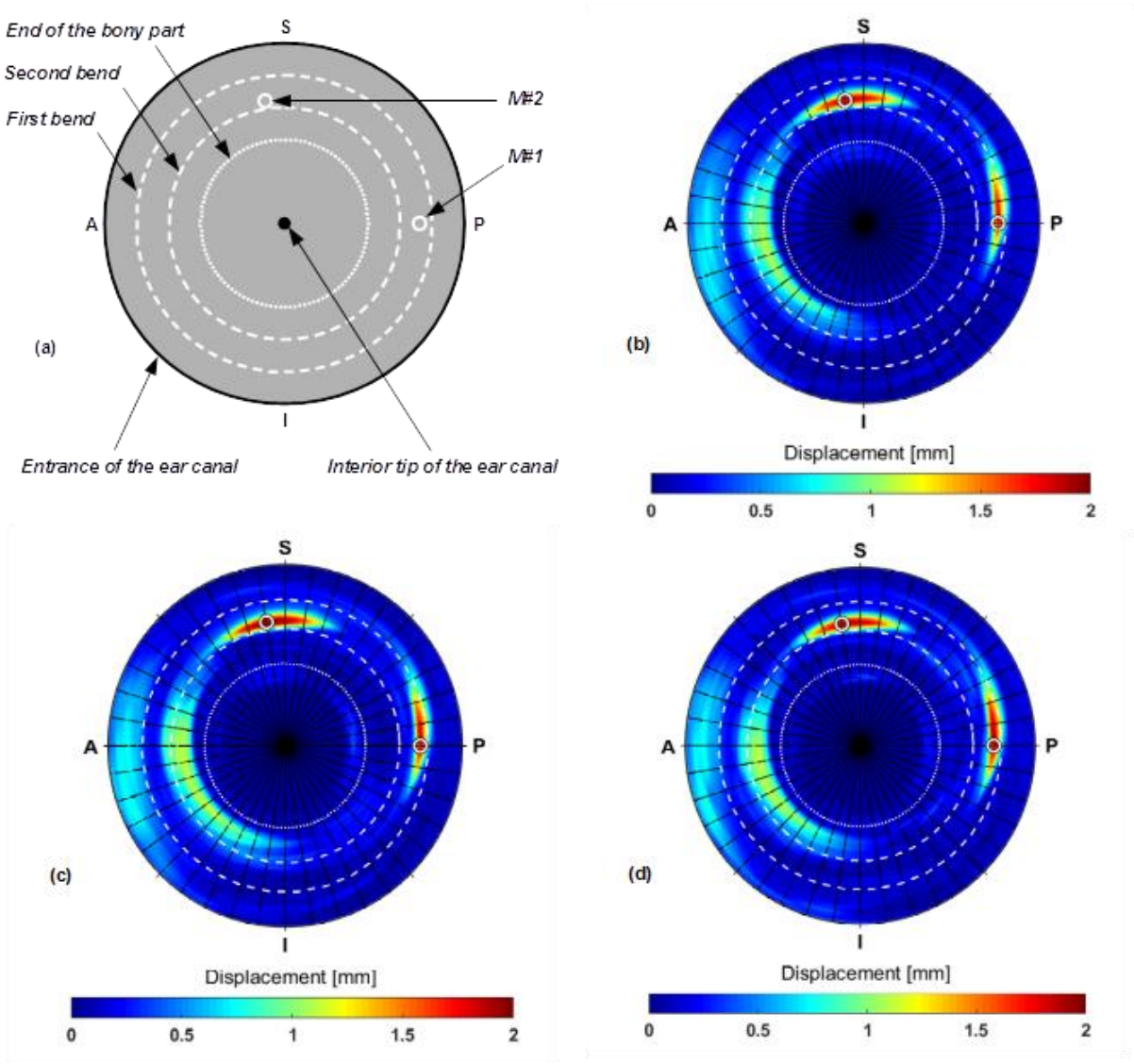

Figure 6: Surface plot of the ear canal walls displacement magnitude using segmentations performed by operator OP#1 (b), OP#2 (c) and OP#3 (d). The legend is given by the first diagram (a) where S, I, A and P indicate the orientation of the cartography and correspond to Superior, Inferior, Anterior and Posterior respectively. The center of the polar plot corresponds to the tip of the ear canal and the largest circle to the entrance of the ear canal. The dashed lines roughly match the position of the first and the second bends of the ear canal. The dotted line matches at the same time the tip of IED#1 and IED#2 and the end of the bony part of the ear canal. The white circles are the locations of the beads manually identified on the target image.

The center of the plot corresponds to the interior tip of the ear canal set as the reference position (0 mm) and the largest circle corresponds to the entrance of the ear canal arbitrarily chosen at 33 mm from the end of the ear canal. Thus, the smaller the circle, the deeper the location in the ear canal. The smallest dotted white circle corresponds to the end of the bony part and the large and small white dashed circles correspond to

the first and second bends respectively. The white circles give the locations of the beads manually identified on the target image.

The location of the maximum displacement is well estimated since the regions of higher displacement correspond to the location of the beads. The first bead is located on the posterior part of the ear canal just after the first bend represented by the largest dashed white circle. The second bead is located on the upper part of the ear canal close to the second bend represented by the smallest dashed white circle. These locations are in agreement with the positions of the beads described in the section 1.1.2. The maximum displacement due to beads is estimated between 1.5 and 2 mm. In order to obtain a precise value of this amplitude, the maximum displacement along the ear canal is plotted in Figure 7.

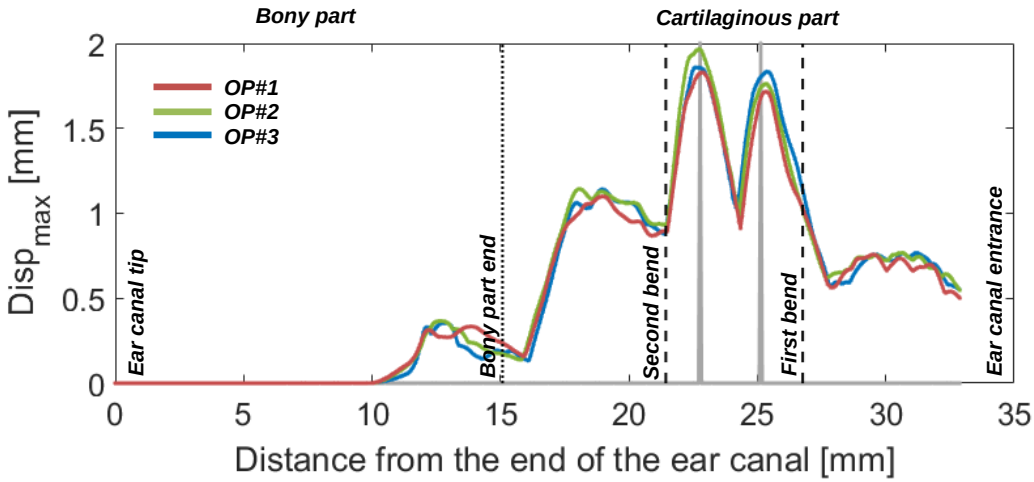

Figure 7: Maximum displacement along the ear canal obtained for operator OP#1 (red), OP#2 (green) and OP#3 (blue). 0 corresponds to the tip of the ear canal and the gray curve gives the locations of the beads manually identified on the target image. The dashed lines roughly match the position of the first and the second bends of the ear canal. The dotted line matches at the same time the tip of IED#1 and IED#2 and the end of the bony part of the ear canal.

The computed maximum displacement along the ear canal is given by the red (OP#1), green (OP#2) and blue (OP#3) curves and is compared to the positions of the centers of beads identified on the target image given by the gray vertical lines. The distances between the beads and the tip of the ear canal are equal to 25.1 and 22.8 mm for the first and second beads respectively. The corresponding mean values of the computed

positions of the beads are 25.4 (stand. dev. = 0.1) and 22.6 (stand. dev. = 0.1) mm. The corresponding errors between the computed and measured bead positions are -0.3 (stand. dev. = 0.1) and + 0.2 (stand. dev. = 0.1) mm respectively. The maximum errors are obtained for OP#1 and equal - 0.4 mm and + 0.2 mm.

The average maximum amplitude of the displacement is equal to 1.8 (stand. dev. = 0.1) and 1.9 (stand. dev. = 0.1) mm for the first and second beads respectively. Since the diameter of both beads equals 1.9 mm, the mean corresponding errors between the computed and measured displacement amplitudes due to beads are + 0.1 (stand. dev. = 0.1) and 0.0 (stand. dev. = 0.1) mm respectively. The maximum errors are obtained for OP#1 and equal + 0.2 mm for both beads. All these results are summarized in Table 6.

	Reference [mm]	**OP#1 [mm]**		**OP#2 [mm]**		**OP#3 [mm]**		**Mean (Stand. Dev.) [mm]**	
		Computed	**Diff.**	**Computed**	**Diff.**	**Computed**	**Diff.**	**Computed**	**Diff.**
Position B#1	25.1	25.5	-0.4	25.3	-0.2	25.4	-0.3	25.4 (0.1)	-0.3 (0.1)
Position B#2	22.8	22.6	+0.2	22.7	+0.1	22.6	+0.2	22.6 (0.1)	+0.2 (0.1)
Diameter B#1	1.9	1.7	+0.2	1.8	+0.1	1.8	+0.1	1.8 (0.1)	+0.1 (0.1)
Diameter B#2	1.9	1.7	+0.2	2.0	-0.1	1.9	0	1.9 (0.1)	0.0 (0.1)

Table 6: Position and amplitude of the computed displacement due to beads for each operator.

It is noteworthy that the bony part of the ear canal is not expected to be deformed by the IED insertion. Thus, the deformable registration focuses only on a part of the ear canal from its entrance to 10 mm before its interior tip. This is why the computed deformation in the beginning of the ear canal from 0 to 10 mm is equal to zero.

In Figures 6 and 7, a third region is deformed by the IED#2. This region is located between the end of the bony part and the second bend of the ear canal and deforms

in the posterior/anterior direction. For this region, the average maximum amplitude is equal to 1.2 (stand. dev. = 0.1) mm and is located at 18.7 (stand. dev. = 0.4) mm from the reference position. This unexpected deformation is due to the pressure of the tip of the IED#2 on the ear canal walls due to a global displacement of the device. Indeed, the hypothesis that the ear canal is only deformed by the beads is not exact. In fact, the rigidity of the silicone mimicking the soft tissues is large enough to shift the position of the IED#2 compared to the initial position of the IED#1. Due to this global displacement, the tip of the IED#2 also deforms the ear canal walls. The effects of this unexpected displacement are discussed in section 3.

The accuracy of the deformable registration step is then evaluated using similarity indices presented in section 1.4.3. First, these indices are computed using the source (ear canal occluded by IED#1) and target (ear canal occluded by IED#2) images and then using the deformed (ear canal occluded by IED#1 deformed by the registration technique) and target (ear canal occluded by IED#2) images. The similarity indices presented in Table 7 are computed only for the region concerned by the deformable registration and located from the entrance to 10 mm before the tip of the ear canal.

	OP#1		**OP#2**		**OP#3**		**Mean (Stand. dev.)**	
	S/T	**D/T**	**S/T**	**D/T**	**S/T**	**D/T**	**S/T**	**D/T**
Dice	0.970	0.994	0.967	0.989	0.964	0.983	0.967 (0.002)	0.989 (0.004)
False negative	0.052	0.007	0.061	0.019	0.065	0.033	0.059 (0.005)	0.020 (0.011)
False positive	0.007	0.005	0.004	0.003	0.005	0.005	0.005 (0.001)	0.003 (0.002)

Table 7: Similarity indices for the source/target (S/T) and deformed/target (D/T) segmentations used for the deformable registration.

The Dice index is clearly higher for the deformed and target segmentations (D/T in Table 7). Moreover, the number of false negatives and false positives decreases after registration. All these results indicate that the registration is accurate since the Dice index is very close to 1 and the false negatives and false positives are very close to 0 after the registration.

2.2.2 Precision

In order to quantitatively evaluate the precision of the deformable registration step, similarity indices computed using the three deformed segmentations are given in Table 8.

	OP#1/OP#2	OP#1/OP#3	OP#2/OP#3	Mean (Stand. dev.)
Dice	0.994	0.989	0.993	0.992 (0.002)
False negative	0.012	0.000	0.002	0.005 (0.005)
False positive	0.001	0.021	0.012	0.011 (0.008)

Table 8: Similarity indices for the segmentations deformed using the transformation file computed during the deformable registration step.

These results show that the deformable registration step is precise since the values of the Dice are close to 1 and the values of false negatives and positives are close to 0.

2.2.3 Registration noise

In order to evaluate the registration noise defined in section 1.4.4, a region considered as fixed after the rigid registration step is chosen in the bony part of the artificial ear. The deformable registration using parameters of Table 3 is applied to this region with the same source and target images as used to compute the ear canal deformation. The maximum displacement obtained using this deformable registration is computed and the maximum value of this estimated displacement represents the registration noise. This noise is dependent on the registration parameters and on the quality of the studied images. The maximum computed displacement is 0.3 mm and the average displacement is 0.2 mm. The registration noise is close to the difference between the manually measured and computed maximum displacement at the position of the beads found in section 2.2.1. Thus, in this case, computed values obtained using the registration method are relevant with an accuracy equal to +/- 0.3 mm.

2.3 Registration for MRI-like resolution images

The registration method is then applied to images with a degraded resolution. The cartography of the computed displacement and the corresponding maximum displacement along the ear canal are given in Figure 8 and 9 respectively.

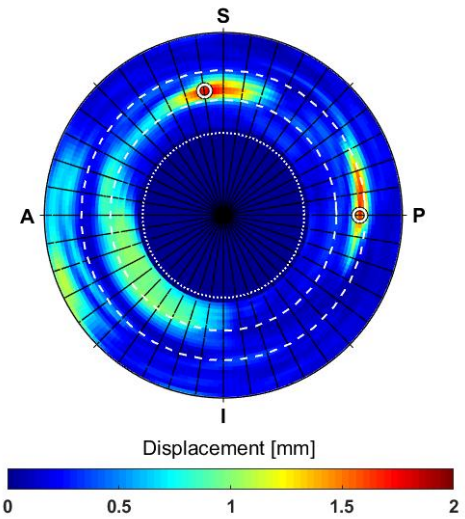

Figure 8: Surface plot of the ear canal walls displacement magnitude due to beads for a MRI-like resolution (0.6 mm isotropic). The S, I, A and P indicate the orientation of the cartography and correspond to Superior, Inferior, Anterior and Posterior respectively. The center of the polar plot corresponds to the tip of the ear canal and the largest circle to the entrance of the ear canal. The dashed lines roughly match the position of the first and the second bends of the ear canal. The dotted line matches at the same time the tip of IED#1 and IED#2 and the end of the bony part of the ear canal. The white circles are the locations of the beads manually identified on the target image.

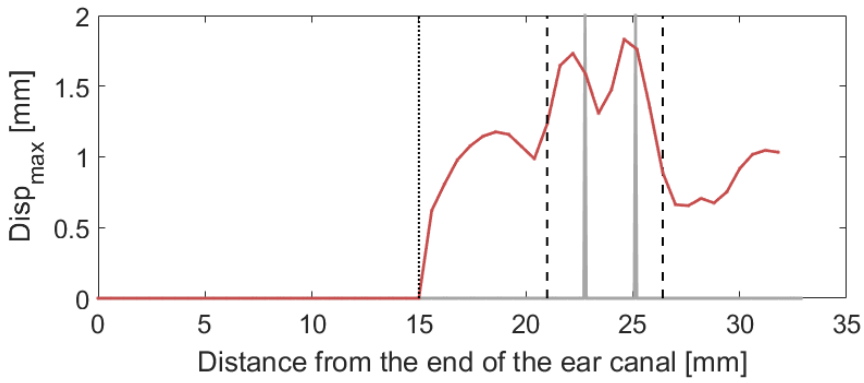

Figure 9: Maximum displacement along the ear canal for a MRI-like resolution (0.6 mm isotropic). The zero corresponds to the tip of the ear canal. The gray vertical lines give the locations of the beads manually identified on the target image and the red curve gives the maximum displacement estimated thanks to the deformable registration. The dashed lines roughly match the position of the first and the second bends of the ear canal. The dotted line matches at the same time the tip of IED#1 and IED#2 and the end of the bony part of the ear canal.

According to Figures 8 and 9, the location and the amplitude of the displacement of the ear canal due to beads computed using degraded images is good enough to give an estimation of the actual displacement. Indeed, the position of the first and second beads is 24.6 mm and 22.2 mm respectively and the amplitude of the corresponding displacement is 1.7 mm for both. These results can be compared to values of Table 6. The differences of location between the measured and computed displacement are +0.5 mm and +0.6 mm for the first and second beads respectively and the difference of amplitude is +0.2 mm for both.

3 Discussion

This section presents a discussion about the reliability of the proposed method for assessing the displacement field of an occluded ear canal from medical images. It can be considered that the displacement obtained using the deformable registration is satisfactorily estimated compared to the expected displacement. The difference observed between the expected and the estimated displacement can be explained by (i) a global displacement of the IED#2 due to the rigidity of the silicone mimicking the soft tissues, (ii) the registration noise which has a maximum value equal to 0.3 mm and (iii) the accuracy and the precision of the segmentation performed by the operator. However, even with these potential error sources, the proposed method is still relevant for the estimation of the displacements inside an ear canal since the computed values are close to the measured ones (see Table 6). The inter-operator variability does not lead to important errors since the similarity between segmentations performed by the three operators is high. The results of the registration step using different segmentations lead to similar results for the estimation of the location and amplitude of the displacement in the ear canal due to beads.

In this paper, the rigid registration step is considered as accurate and precise. Although the error due to this registration step seems very small since the mismatch between

the source and target images is not visually observable, another source of error can change the accuracy and precision of the overall method. During registration, the voxel gray values of the moved image are interpolated to match the gray values of the target image. This interpolation slightly modify the moved image adding an inherent source of error for the next registration step. In this study, this error is considered as small since the histograms of the gray values for the source and moved images are very similar.

It is worth mentioning that only one deformable registration model with one set of input parameters has been applied in this paper. These parameters have been chosen using a trial and error method driven by the characteristics of the images (e.g. the resolution for the shrink factor or the order of magnitude of the displacement for the transformation model). The precision of the registration highly depends on these parameters and a great attention should be paid to choose them. The visual inspection of the deformed image compared to the target image is essential to verify that the chosen parameters give a precision good enough to correctly estimate the displacement field due to IED insertion.

For the deformable registration step, other metrics, simpler and with lower computation cost than the cross correlation metric, could have been used. However, one of the future aim of this work is to apply the proposed method to MR images of human ear canals. To ensure the possibility to apply this method to the greatest number of cases, the robustness of the cross correlation metric is preferred to the simplicity of other metrics in this study.

Another important point to underline deals with the artificial ear used to validate the method. The final objective of this research is to apply the proposed method to assess the displacement of human subjects' ear canals due to the insertion of any IED. Images obtained on human subjects are more complex than images used in this paper due to

the diversity of human biologic tissues (e.g. muscles, fat and skin for soft tissues, cortical or trabecular parts for bones). However, if an expert operator is able to segment both the air inside the ear canal and the IED, the proposed method is still relevant for the estimation of the displacement in a real ear canal.

The last point to discuss is about the estimation of the ear canal displacement field using images with a MRI-like resolution. According to the results of section 2.3, only the location of the beads is impacted by the images degradation. However, this error could be decreased using image post-processing like oversampling or non local mean filtering to obtain a finer estimation of the bead positions. These results show that the proposed method is promising for an application to MR images.

4 Conclusion

This paper proposes a method to estimate the displacement field inside the ear canal due to in-ear device insertion. This method was validated on an artificial outer ear made with a geometry and materials mimicking a real ear. First, CT images were used to obtain the geometry of the artificial ear canal occluded by two different IEDs with controlled shapes. The shape difference between these two IEDs is due to beads added to the first device referred to as IED#1 to obtain the second device referred to as IED#2. A registration method was applied to compute the displacement field due to the insertion of the IED#2 compared to the insertion of the IED#1. To avoid registration errors, occluded ear canals have been segmented. The accuracy and the precision of the proposed method were tested for images segmented by three operators. Results showed that the proposed method is able to satisfactorily estimate the location and the amplitude of the deformation inside the ear canal due to beads. The inter-operator segmentation variability affects slightly this estimation but not enough to be significant. Preliminary results on images with a degraded resolution also gave similar results. Future works will investigate the potential of the proposed method in order to obtain

the displacement field of the ear canal of a human subject due to IED insertion using MR images.

Acknowledgements

Authors want to thanks the Laboratoire Auditif Laviolette from Trois-Rivières for the custom earplug, Bruno Jetté for his help with the CT acquisitions, Huiyang Xu and Thomas Padois for their time spent in the segmentation process and the IRSST for the funding of this research (grant number 2016-0020).

References

(Avants, et al., 2008), Avants, B.B., Epstein. C.L., Grossman, M., Gee, J.C., “Symmetric diffeomorphic image registration with cross-correlation: Evaluating automated labeling of ederly and neurodegenerative brain”, Medical Image Analysis, 12, p. 26-41, 2008

(Avants, et al., 2011), Avants, B.B., Tustison, N.J., Song, G., Cook, P.A., Klein, A., Gee, J.C., “A reproducible evaluation of ANTs similarity metric performance in brain image registration”, NeuroImage, 54, p. 2033-2044, 2011

(Azeres, et al., 2008), Arezes, P.M., Abelenda, C., Braga, A.C., “An evaluation of comfort afforded by Hearing Protection Devices”, Proceedings of the AHFE 2008: 2nd International Conference on Applied Human Factors and Ergonomics, p. 1-8, Las Vegas, USA, 14-18 July, 2008

(Baker, et al., 2010), Baker, A.T., Lee, SH., Mayfield, F., “Evaluating Hearing Protection Comfort Through Computer Modeling”, Proceedings of the 2010 Simulia customer conference, Providence, Rhode Island, USA, May 25-27, 2010

(Carioli, et al., 2016), Carioli, J., Delnavaz, A., Zednik, R.J., Voix, J., “Power capacity from earcanal dynamic motion”, AIP Advances, 6(12), p. 1-10, 2016

(Casali, et al., 1987), Casali, J.G., Lam, S.T., Epps, B.W., “Rating and Ranking Methods for Hearing Protector Wearability”, Sound and vibration, 21(12), p. 10-18, December 1987

(Conrad, et al., 2013), Conrad, S., Rout, A., “Perceived occlusion and comfort in receiver-in-ear hearing aids”, American Journal of Audiology, 22, p. 283-290, 2013

(Darkner, et al., 2007), Darkner, S., Larsen, R., Paulsen, R.R., “Analysis of Deformation of the Human Ear and Canal Caused by Mandibular Movement”, In: Ayache N., Ourselin S., Maeder A. (eds) Medical Image Computing and Computer-Assisted Intervention – MICCAI 2007. MICCAI 2007. Lecture Notes in Computer Science, vol 4792. Springer, Berlin, Heidelberg

(Darkner, et al., 2008), Darkner, S., Sabuncu, M.R., Golland, P., Paulsen, R.R., Larsen, R., “Analysis of surfaces using constrained regression models”, Med Image Comput Comput Assist Interv, 11, p. 842-849, 2008

(Darkner, et al., 2017), Darkner, S., Jonsson, S., Sommer, S., “In vivo study of the human ear canal using contrast-enhanced MRI”, 25th Annual Meeting of the International Society for Magnetic Resonance in Medicine, Hawaii, USA, 2017

(Davis, et al., 2008), Davis, R.R., “What do we know about hearing protector comfort?”, Noise and Health, 10 (40), p. 83, 2008

(Davis, et al., 2016), Davis, R.R., Shaw, P.B., “Hearing protector comfort and Personal Attenuation Ratings: A real world study,” San Diego, CA, USA, 2016

(Delnavaz, et al., 2013), Delnavaz, A., Voix, J., “Ear canal dynamic motion as a source of power for in-ear devices”, Journal of Applied Physics, 113(064701), p. 1-8, 2013

(Delnavaz, et al., 2014), Delnavaz, A., Voix, J., “Energy Harvesting for In-ear Devices Using Ear Canal Dynamic Motion”, IEEE Transactions on Industrial Electronics, 16(1), p. 583-590, 2014

(Doutres, et al., 2017), Doutres, O., Sgard, F.C., Terroir, J., “A review about hearing protection comfort and its evaluation”, Proceedings of Acoustics’17 Boston, 173rd Meeting of the Acoustical Society of America and the 8th Forum Acusticum, Boston MA, 25-29 June, 2017

(Egolf, et al., 1993), Egolf, D.P., Nelson, D.K., Howell, H.C. III, Larson, V.D., “Quantifying ear-canal geometry with multiple computer-assisted tomographic scans”, The Journal of the Acoustical Society of America, 93(5), p. 2809-2819, 1993

(French-Saint, et al., 1978), French-Saint, G.M., Barr-Hamilton, R.M., “Relief of the occluded ear sensation to improve earmold comfort”, Journal of the American Audiology Society, 4(1), p. 30-5, 1978

(Grenness, et al., 2001), Grenness, M.J., Osborn, J., Weller, W.L., “Mapping ear canal movement using area-based surface matching”, The Journal of the Acoustical Society of America, 111(2), p. 960-971, 2001

(Harrison, 1993), Harrison, C., “Hearing Protection attenuation. Is more really better?”, OH&S Canada, Buyer’s guide, 1993

(Inoue, et al., 2011), Inoue, J., Yamashita, Y., Horie, S., Kawanami, S., Takahashi, K., “Earplug fitting and the computed tomography”, Proceedings of Internoise 2011, Osaka, Japan, p. 1-10, 2011

(Klein, et al., 2009), Klein, A., Andersson, J., Ardekani, B.A., Ashburner, J., Avants, B., Chiang, M.C., Christensen, G.E., Collins, D.L., Gee, J., Hellier, P., Song, J.H., Jenkinson, M., Lepage, C., Rueckert, D., Thompson, P., Vercauteren, T., Woods, R.P., Mann, J.J., Parsey, R.V., “Evaluation of 14 nonlinear deformation algorithms applied to human brain MRI registration”, NeuroImage, 46, p. 786-802, 2009

(Kochkin, 2000), Kochkin, S., “MarkeTrak V: ”Why my hearing aids are in the drawer”: The consumers' perspective”, The Hearing Journal, 53(2), p. 34-41, February, 2000

(MacKenzie, et al., 1989), MacKenzie, K., Browning, G.G., McClymont, L.G., “Relationship between earmould venting, comfort and feedback”, British Journal of Audiology, 23, p. 335-337, 1989

(Norris, et al., 2012), Norris, J., Chambers, R., Kattamis, N., Davis, B., Bieszczad, J., “Effects of Custom Earplug Design Parameters on Achieved Attenuation”, Poster presentation at the annual meeting of the National Hearing Conservation Association, New Orleans, LA, USA, 2012

(Oliveira, 1997), Oliveira, R.J., “The Active Earcanal”, Journal of the American Academy of Audiology, 8, p. 401-410, 1997

(Park, et al., 1991), Park, M.Y., Casali, J.G., “An Empirical Study of Comfort Afforded by Various Hearing Protection Devices: Laboratory versus Field Results”, Applied Acoustics, 34, p. 151-179, 1991

(Pirzanski, et al., 2004), Pirzanski, C., Berge, B., “If you blame buffing for bad fittings, you’ve probably given the wrong impression”, The Hearing Journal, 57(2), p. 40-45, 2004

(Stinson, et al., 1989a), Stinson, M.R., Lawton, B.W., “Specification of the geometry of the human ear canal for the prediction of sound-pressure level distribution”, The Journal of the Acoustical Society of America, 85(6), p. 2492-2503, 1989

(Stinson, et al., 1989b), Stinson, M.R., Khanna, S.M., “Sound propagation in the ear canal and coupling to the eardrum, with measurements on model systems”, The Journal of the Acoustical Society of America, 85(6), p. 2481-2491, 1989

(Yu, et al., 2015), Yu, J.F., Lee, K.C., Wang, R.H., Chen, Y.S., Fan, C.C., Peng, Y.C., Tu, T.H., Chen, C.I., Lin, K.Y., “Anthropometry of external auditory canal by non-contactable measurement”, Applied Ergonomics, 50, p. 50-55, 2015

(Zitova, et al., 2003), Zitova, B., Flusser, J., “Image registration methods: a survey”, Image and Vision Computing, 21, p. 977-1000, 2003